

X-ray magnetic circular dichroism in CeFe₂: First-principles calculations

V. N. Antonov,^{1,2} D. A. Kukusta,² and A. N. Yaresko¹

¹Max-Planck-Institut für Festkörperforschung, Heisenberg Strasse 1, D-70569 Stuttgart, Germany

²Institute of Metal Physics, 36 Vernadsky Street, 03142 Kiev, Ukraine

(Received 8 May 2008; revised manuscript received 27 June 2008; published 4 September 2008)

The x-ray magnetic circular dichroism (XMCD) spectra of CeFe₂ at the Ce $L_{2,3}$, $M_{4,5}$, Fe K , and $L_{2,3}$ edges are investigated theoretically from first principles, using the fully relativistic Dirac linear muffin-tin orbital band-structure method. The electronic structure is obtained with the local spin-density approximation. The origin of the XMCD spectra in the compound is examined. The core hole effect in the final states has been investigated using a supercell approximation. It improves the agreement between the theory and the experiment at the Ce M_5 edge. However, it has a minor influence on the shape of the Ce $L_{2,3}$ XMCD spectra.

DOI: 10.1103/PhysRevB.78.094401

PACS number(s): 75.50.Cc, 71.20.Lp, 71.15.Rf

I. INTRODUCTION

In rare-earth compounds, where $4f$ levels are relatively close to the Fermi energy, various anomalous phenomena frequently appear. Most of them can be attributed to the hybridization between the $4f$ states and conduction bands. The great interest for the electronic and magnetic structures in compounds formed between rare-earth (R) and transition metals (T) has been recognized for a long time. However, among the R , cerium is somehow a controversial element. In cerium metal the $4f$ states are at the borderline between localized and itinerant behavior. This is reflected in a remarkable transition from the fcc γ phase with localized $4f$ configuration into the isostructural α phase with delocalized $4f$ configuration. The transition may be driven thermally, by the application of pressure or by alloying and formation of compounds with d -band transition metals, and is initially related to a varying degree of mixing of the $4f$ and conducting states—i.e., to the formation of highly correlated electronic structure.

Among the Ce- T series the C15 Laves phase compounds, CeT₂ (T =Ni, Co, and Fe), which stand out as archetype of the α -Ce class, have been studied intensively.¹

CeFe₂ compound presents a strong anomaly in physical properties in comparison with other R Fe₂ compounds, which originates from $3d$ - $4f$ hybridization. First, there is a strong reduction in the lattice parameter in comparison with the expected smooth decrease through the R Fe₂ series, leading to a lattice constant for CeFe₂ as small as that for HoFe₂. Second, the magnetic properties present characteristic features. The Curie temperature ($T_c=230$ K) is depressed by a factor of nearly 3 as compared to LuFe₂ ($T_c=610$ K, La-Fe compounds do not exist). The magnetic moments are also anomalously low ($\mu_{Fe}\approx 1.4 \mu_B$ and $\mu_{Ce}\approx 0.7 \mu_B$, coupled antiferromagnetically to each other). The saturation magnetization is equal to $2.30 \mu_B/f.u.$, the magnetic susceptibility follows the Curie-Weiss law with an effective moment of $7.4 \mu_B/f.u.$ (Ref. 2). Moreover, magnetic and neutron-diffraction studies have shown that the substitution of small amount (only a few percent) of Fe by Co, Al, Si, or Ru reveals a second magnetic transition with an abrupt loss of ferromagnetism at Neel temperature T_N , lower than the bulk ordering temperature T_c . In particular, with Co substitution

an antiferromagnetic phase appears for $T\leq 80$ K.³ From recent neutron-scattering experiments for CeFe₂, Paolasini *et al.*⁴ reported that there is an AFM spin fluctuation with a propagation vector $\mathbf{q}=(\frac{1}{2}, \frac{1}{2}, \frac{1}{2})$ below about 100 K even in the FM state. They also revealed that the AFM spin fluctuation with the same \mathbf{q} vector exists in the FM state for Ce(Fe_{0.93}Co_{0.07})₂ and that it changes into a typical AFM spin wave in the AFM state at low temperatures.⁵ The AFM spin fluctuation and the AFM spin wave observed by them are associated with the Fe spins. They also showed that the AFM state of Ce(Fe_{0.93}Co_{0.07})₂ is not a simple collinear AFM structure but a noncollinear one. From magnetization measurements using a CeFe₂ single crystal, Fukuda *et al.*⁶ revealed that the magnetization along the $\langle 111 \rangle$ direction at 5 K is anisotropically suppressed by applying hydrostatic pressure. According to their conclusion, such an anisotropic suppression of the magnetization originates from the anisotropic Ce $4f$ -Fe $3d$ hybridizations with a strong magnetoelastic effect. Fujiwara *et al.*⁷ carried out the magnetization measurements of single-crystal CeFe₂ under hydrostatic pressures up to 8 kbar and showed that the magnetization was quite anisotropically suppressed at 5 K even in a cubic symmetry by applying the hydrostatic pressure, while the neutron-diffraction studies indicate that the antiferromagnetic spin fluctuation with a propagation vector $\mathbf{q}=(\frac{1}{2}, \frac{1}{2}, \frac{1}{2})$ was enhanced by applying hydrostatic pressure of 15 kbar.

All anomalous physical properties of CeFe₂ suggest that the Ce $4f$ states in CeFe₂ hybridize strongly with the other valence electrons, notably the Fe $3d$ valence states.¹

The band-structure investigations of the CeFe₂ were carried out by several authors.^{8–11} Already first band-structure calculation by Eriksson *et al.*⁸ using the linear muffin-tin orbital (LMTO) method within atom sphere approximation (ASA) shows that total magnetic moments at the Fe and Ce sites are aligned antiferromagnetically. It was an indication on itinerant character of the $4f$ states in CeFe₂. The relativistic effect was found to be relatively small. Trygg *et al.*¹⁰ provided the energy-band-structure calculations of CeFe₂ including spin-orbit (SO) coupling and orbital polarization using the full potential linear muffin-tin orbital (FP-LMTO) method. Later on Konishi *et al.*¹¹ obtained similar results using also the FP-LMTO. The Ce $4f$ electrons were treated as itinerant band electrons. They also reported on results

from high-energy spectroscopic measurements using core-level and valence-band photoemissions, inverse photoemission, and soft x-ray absorption techniques. It was found that the Ce $4f$ partial density of states (DOS) obtained from the band-structure calculations agrees well with the experimental spectra concerning both the $4f$ peak position and the $4f$ bandwidth if the surface effects are properly taken into account. The combined analyses of the experimental and theoretical results indicate a very strong hybridization of the Ce $4f$ states with the delocalized band states, mainly the Fe $3d$ states.

In the present study, we focus our attention on the theoretical investigation of the x-ray magnetic circular dichroism (XMCD) in CeFe₂ compound. Actually XMCD is one of the most promising techniques to reveal local electronic and magnetic properties in a variety of magnetic materials essentially because of its element as well as shell selectivities. In fact, with the help of circular polarized x-rays of good quality, arising from third generation synchrotron facilities, a lot of data have been accumulated up to now on x-ray absorption spectroscopy (XAS) and XMCD of transition-metal and rare-earth compounds.

The first experimental XMCD measurements of CeFe₂ at the Ce $M_{4,5}$ absorption edges were carried out by Schille *et al.*¹² The uncertainty of these experiments was too large to allow a reliable quantitative determination of the absolute value of the local $4f$ moments on Ce. Later, using high quality sample and better experimental conditions Delobbe *et al.*¹³ measured the x-ray magnetic circular dichroism at the Fe $L_{2,3}$, Ce $M_{4,5}$, and Ce $L_{2,3}$ absorption edges of CeFe₂. Application of the sum rules yields both the magnitude and the direction of the magnetic contributions to the total moment in CeFe₂. A total Ce magnetic contribution of $-0.29\mu_B$ ($M^{5d}=-0.13\mu_B$, $M^{4f}=-0.16\mu_B$) and a ratio for the $4f$ contribution $\langle L_z \rangle / \langle S_z \rangle \approx -1$ were found, which confirmed that the $4f$ states are highly hybridized in CeFe₂. The experimental results of XAS and XMCD spectra for CeFe₂ at the Ce $L_{2,3}$ and Fe K absorption edges were presented in Refs. 3 and 12. Mizumakia *et al.*¹⁴ measured Ce $L_{2,3}$ XMCD spectra in Ce(Fe_{1-x}Co_x)₂ compounds for $x=0.0, 0.2$, and 0.3 . Klose *et al.*¹⁵ investigated the magnetic circular dichroism on Ce/Fe multilayers at the Fe K and Ce $L_{2,3}$ absorption edges.

As for the XMCD and photoemission spectroscopy (PES) studies of R compounds, it is widely believed that the spectra are well described by the single impurity Anderson model (SIAM).^{16,17} Indeed during many years Kotani's group demonstrated a remarkable agreement between theoretically calculated and the experimentally measured XMCD spectra in the rare-earth compounds with different degrees of the $4f$ localization using the SIAM approximation.¹⁸⁻²² To describe the hybridization of R $5d$ states with spin polarized transition-metal $3d$ states of surrounding ions, they used a cluster model. The method contains several adjustable parameters (such as the energy of the $4f$ level, ϵ_{4f} , Coulomb interaction between the $4f$ electrons, U_{ff} , and between $4d$ and $5d$ states, U_{fd} , core-hole potentials U_{fc} and U_{dc} , and hybridization parameter between $4f$ and conducting states V_{fd}). By proper choice of these parameters, they were able to describe quite well the shape of the R XMCD spectra at the $L_{2,3}$ edges for the considered series of R -T, including CeFe₂

compound (see review paper²³). Recently, however, it has been argued that for systems in which the Ce $4f$ states hybridize strongly with the other valence electrons, calculations based on the density-functional theory (DFT) may give an equally good or even better description of the PES and XMCD spectra than the SIAM analysis.^{11,24,25} However, one should bear in mind that calculations based on DFT are not strictly applicable for excited state properties—in contrast to the ground-state properties, such as the magnetic moments of the ground state, which are typically the focus of these calculations. Nevertheless, the electronic structure obtained from such calculations is often compared with photoemission or XMCD data, and a good agreement between experiment and calculations is frequently observed. In the limit of the complete screening of the excited state, one would expect the ground-state density-functional calculations to be able to describe the spectra well. Still there are only a few *ab initio* calculations of the XMCD spectra in rare-earth compounds²⁶⁻³⁰ and no such calculations for the CeFe₂ compound in literature.

This paper is organized as follows: Section II presents a description of CeFe₂ crystal structure as well as the computational details. Section III is devoted to the electronic structure and XMCD spectra of CeFe₂ calculated with the fully relativistic Dirac LMTO band-structure method. The calculated results are compared with the available experimental data. Finally, the results are summarized in Sec. IV.

II. CRYSTAL STRUCTURE AND COMPUTATIONAL DETAILS

CeFe₂ crystallizes in the cubic $Fd\bar{3}m$ structure (space-group 227) and belongs to the large class of C15 Laves phase compounds. The unit cell consists of two formula units (i.e., six atoms) with a lattice constant $a=7.3$ Å.³¹ Ce ions occupy the $8a$ Wyckoff positions ($x=0, y=0, z=0$). Fe ions occupy the $16d$ positions ($x=\frac{5}{8}, y=\frac{5}{8}, z=\frac{5}{8}$). The Ce atoms have 12 Fe atoms as nearest neighbors (at 3.0265 Å distance), while for Fe there are six Fe atoms (at 2.581 Å distance) and six Ce atoms (at 3.0265 Å distance).

The details of the computational method are described in our previous papers,^{32,33} and here we only mention several aspects. The calculations have been performed using the spin-polarized LMTO method^{34,35} with the combined correction term taken into account. We used the Perdew-Wang³⁶ parametrization for the exchange-correlation potential. Brillouin zone (BZ) integrations were performed using the improved tetrahedron method³⁷ and charge self-consistently was obtained with 349 irreducible \mathbf{k} points. The basis consists of Ce s, p, d , and f ; Fe s, p , and d LMTOs.

In order to simplify the comparison between calculated and experimental x-ray absorption spectra phenomenological background intensity was added to the calculated XAS. The background spectra are caused by different kinds of inelastic scattering of the electrons promoted to the conduction band above the Fermi level (scattering on potentials of surrounding atoms, defects, phonons, etc.). The problem is also well known in x-ray photoemission spectroscopy. The calculation of these processes from first principles is extremely difficult

and has not been solved properly up to now. However, the background spectrum can be easily described phenomenologically.^{38,39} In the present work the background intensity was approximated using a simple method describe in our previous paper.³² A similar procedure was proposed by Röhler.⁴⁰

It should also be mentioned that at photon energies far above the absorption edge the states with the next principal quantum number—e.g., Fe $4d$ and Ce $5d$ states in the case of absorption at the Fe and Ce $L_{2,3}$ edge, respectively—contribute appreciably to the final-state wave function. As these states were not included into the LMTO basis set, the absorption intensity at high photon energies is underestimated in the calculations. The inclusion of the phenomenological background contribution compensates, at least to some extent, for this lack of the calculated XAS intensity.

The finite lifetime of a core hole was accounted for by folding XMCD spectra with a Lorentzian. The widths of K , L_2 , L_3 , M_4 , and M_5 core-level spectra, with $\Gamma_{L_2}=3.41$ eV, $\Gamma_{L_3}=3.19$ eV $\Gamma_{M_4}=0.72$ eV, and $\Gamma_{M_5}=0.72$ eV for Ce; $\Gamma_K=1.19$ eV, $\Gamma_{L_2}=1.14$ eV, and $\Gamma_{L_3}=0.41$ eV for Fe were taken from Ref. 41.

III. RESULTS AND DISCUSSION

A. Energy-band structure

The fully relativistic spin-polarized total and partial DOS of cubic ferromagnetic CeFe₂ are presented in Fig. 1 for the local spin-density approximation (LSDA) approximation. The results agree well with previous band-structure calculations.^{8,10,11}

There is a visible Ce $4f$ -Fe $3d$ as well as Ce $4f$ -Ce $5d$ hybridization at 0 to 2 eV above the Fermi level. The Ce $5d$ empty states possess two major peaks at around 3 and 7 eV above the Fermi level. As we will see later these two peaks are responsible for the double structure of the Ce XAS at the $L_{2,3}$ edges.

A large magnetic moment at the Fe site induces spin splitting of the itinerant Ce $5d$ and Ce $4f$ states through exchange and hybridization effects. From our LSDA calculations, it has been deduced that the total moment $\mu=2.253$ μ_B /f.u. [experimental saturation magnetization is 2.30 μ_B (Ref. 11)] is the result of the antiparallel coupling between Fe (1.473 μ_B) and cerium moments (-0.693 μ_B). The total Ce moment corresponds to a $4f$ contribution of -0.275 μ_B and a $5d$ contribution of -0.221 μ_B . The orbital Ce $4f$ moment was calculated to be 0.151 μ_B . The spin and orbital Fe $3d$ moments are 1.502 μ_B and 0.064 μ_B , respectively.

The LSDA calculations show an unusual antiparallel magnetic coupling between R and transition-metal moments. The experimental evidence of an ordered Ce moment in CeFe₂ antiferromagnetically aligned with respect to the Fe moments was obtained from powder neutron-diffraction experiments.⁴² A few years later, a combination of polarized and unpolarized neutron-diffraction measurements on a CeFe₂ single crystal⁴³ confirmed the previous results obtained on powder samples. The partial magnetic moments in CeFe₂ have been studied also, using Compton scattering⁴⁴

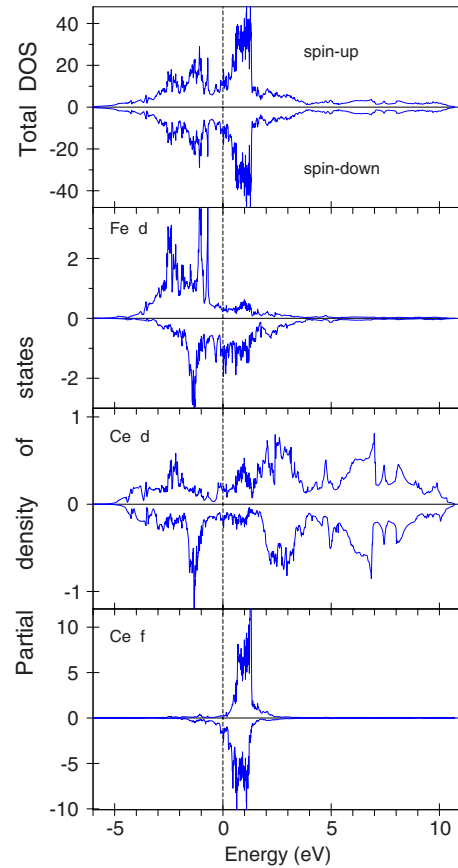


FIG. 1. (Color online) The total [in states/(cell eV)] and partial [in states/(atom eV)] density of states of CeFe₂. The Fermi energy is at zero.

and x-ray magnetic circular dichroism.¹³ In all experiments, an antiparallel coupling of the Ce and Fe moments is found. This coupling is also reproduced in our calculation, as well as in earlier calculations.^{8,10,11} The antiparallel coupling of the moments is a strong indication that the Ce $4f$ states in CeFe₂ are delocalized. Indeed, in CeFe₂, Fe $4d$ and Ce $5d$ states strongly hybridize to form bonding and antibonding bands. When a moment develops at the Fe sites, the energy of spin-up $3d$ states is lowered—reducing the $3d$ - $5d$ hybridization for the spin-up states. The opposite effect occurs for the spin-down states, and the induced Ce $5d$ spin moment is therefore antiparallel to the Fe $3d$ spin moment.⁸ The hybridization between the Fe $3d$ and Ce $5d$ states is more pronounced in the minority channel (see Fig. 1). When a Ce $4f$ electron is localized, the direction of the $4f$ spin moment is dictated by the polarization of the $5d$ electrons so that the Ce and Fe spin moments are always antiparallel. In a Ce³⁺ ion with the f^1 configuration, the $4f$ spin moment is accompanied by an orbital moment—which is larger than the spin moment—and according to Hund's third rule, is antiparallel to it. Hence, for the localized $4f$ electrons the coupling of the total Ce and Fe moments is ferromagnetic. When the Ce $4f$ orbital moment is quenched due to band formation, the coupling becomes antiparallel. It should be mentioned that our band-structure calculations for CeFe₂ show that the Ce spin moment is partially induced by the direct Ce $4f$ -Fe $3d$ hy-

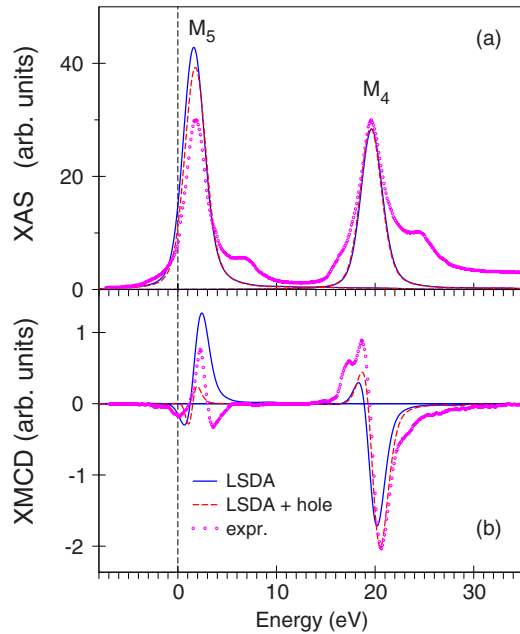


FIG. 2. (Color online) (a) Isotropic absorption spectra of CeFe_2 at the Ce $M_{4,5}$ edges calculated by the LSDA approximation without (full lines) and with taking into account the core-hole effect (dashed lines) in comparison with the experimental data (Ref. 13) (circles). Experimental spectra were measured with external magnetic field (1 T) at 10 K; (b) experimental (Ref. 13) (circles) XMCD spectra of CeFe_2 at the Ce $M_{4,5}$ edges in comparison with theoretically calculated ones using the LSDA approximation without (full lines) and with (dotted lines) taking into account core-hole effect.

bridization, which is an additional argument in favor of the delocalized character of the Ce $4f$ electrons.

B. XMCD spectra

1. Ce $M_{4,5}$ XMCD spectra

The study of the $4f$ electron shell in rare-earth compounds is usually performed by tuning the energy of the x-ray close to the $M_{4,5}$ edges of rare earth where electronic transitions between $3d_{3/2,5/2}$ and $4f_{5/2,7/2}$ states are involved. Figure 2 shows the calculated XAS and XMCD spectra in the LSDA approximation for CeFe_2 at the $M_{4,5}$ edges together with the corresponding experimental data.¹³ The experimentally measured dichroism is large, as is common for R -based systems at the $3d$ threshold.

The theoretically calculated XAS spectra have a rather simple line shape composed of two white line peaks at the M_5 and M_4 edges. However the experimentally measured spectra have a well-known satellite 5 eV above the main lines.¹³ It was not produced by the theory because the multiplet structure has not been included in present calculations.

From Fig. 2(a) one can see that the theory does not reproduce the experimentally observed M_5/M_4 XAS branching ratio. It is well known that in early $3d$ and $4f$ metals with nearly empty $3d$ and $4f$ bands the $L_{2,3}$ and $M_{4,5}$ absorption channels are strongly coupled through the photoelectron core-hole Coulomb and exchange interactions.^{45–48} This leads to a branching ratio 1:1, far from the statistical ratio 2:1

and 3:2 for the L_3/L_2 and M_5/M_4 , respectively—which is obtained in a single-particle theory—unless the spin-orbit interaction in the final $3d$ or $4f$ band is considered. From our relativistic band-structure calculations we obtained the M_5/M_4 branching ratio of 1.42.

We investigate the core-hole effect in the final state using the supercell approximation. When the $3d$ core electron is photoexcited to the unoccupied $4f$ states, the distribution of the charge changes to account for the created hole. To check the convergence of XAS and XMCD spectra for the impurity site, we used supercell calculations with two and four formula units. Very similar spectra were obtained in both cases. The final-state interaction gives the M_5/M_4 branching ratio of 1.34, which is in better agreement with the experimental ratio.

As can be seen from Fig. 2(b) the LSDA approximation describes quite well the shape of the XMCD spectra at the Ce $M_{4,5}$ edges. However it slightly overestimates the intensity of the dichroic signal at the M_5 edge and underestimates it at the M_4 one. It also fails to obtain small negative fine structure observed at the high-energy part of the M_5 XMCD spectrum. The XMCD at the M_4 edge possesses an additional small positive lobe at the low-energy side, which is not in the theoretical calculations. The final-state interaction improves the agreement between theory and the experiment at the M_4 edge; however it underestimates the dichroism at the Ce M_5 edge.

2. Ce $L_{2,3}$ XMCD spectra

For various ferromagnetic Ce intermetallic compounds, x-ray absorption spectra and their x-ray magnetic circular dichroism have been extensively studied for Ce $L_{2,3}$ edges.²³ According to experimental observations, both XAS and XMCD spectra for strongly mixed-valence Ce compounds, which also includes CeFe_2 exhibit a double-peak structure. According to the atomiclike consideration the two peaks in the XAS are associated with a mixed-valence state in CeFe_2 : in the presence of the hole at the core level the lower-energy peak corresponds to the $4f^1 5d^n$ configuration and the higher-energy peak to the $4f^0 5d^{n+1}$ configuration. One should mention, however, that Ce $5d$ states in CeFe_2 have definitely a band character extended at more than 15 eV (see Fig. 1). Therefore one would expect that the calculations based on density-functional theory may give an equally good or even better description of the R XAS and XMCD spectra at the $L_{2,3}$ edge than the atomiclike SIAM analysis.

The XMCD spectra at the Ce $L_{2,3}$ edges are mostly determined by the strength of the SO coupling of the initial Ce $2p$ core states and spin-polarization of the final empty $5d_{3/2,5/2}$ states, while the exchange splitting of the Ce $2p$ core states as well as the SO coupling of the $5d$ valence states are of minor importance for the XMCD at the Ce $L_{2,3}$ edges of CeFe_2 . A qualitative explanation of the XMCD spectra shape can be provided by the analysis of the corresponding selection rules, orbital character, and occupation numbers of individual $5d$ orbitals (see detailed analysis in Ref. 29).

The LSDA approximation reasonably well describes the shape of the XAS and XMCD spectra at the Ce $L_{2,3}$ edges (Fig. 3); however it slightly overestimates the first low-

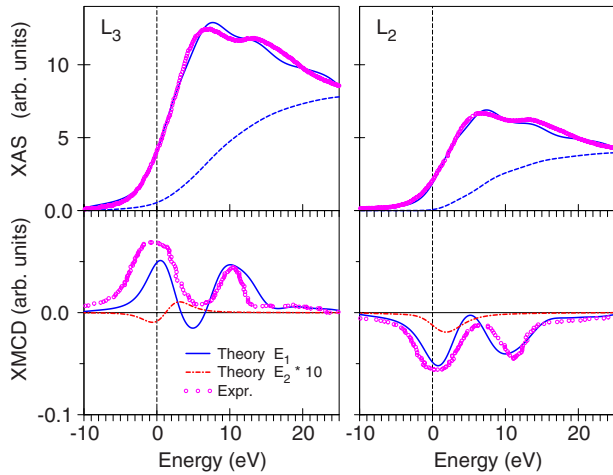


FIG. 3. (Color online) (upper panel) The experimental (Ref. 14) (circles) and theoretical results calculated with the LSDA approximation (full lines) isotropic absorption spectra of CeFe₂ at the Ce $L_{2,3}$ edges. Dashed lines show the background spectra; (lower panel) experimental (Ref. 14) (circles) XMCD spectra of CeFe₂ at the Ce $L_{2,3}$ edges in comparison with the ones calculated using the LSDA (full lines) approximation; the dashed-dotted lines show the contribution from the quadrupole E_2 ($2p \rightarrow 4f$) transitions multiplied by a factor of 10.

energy peak and underestimates the intensity of the dichroic signal between two positive peaks of the L_3 XMCD spectrum.

We found minor influence of the final-state interaction on the shape of the Ce $L_{2,3}$ XMCD spectra in the whole energy interval. A small core-hole effect might come from the fact that the Ce $5d$ states are less localized in comparison with the $4f$ states and have smaller amplitude inside the MT sphere and thus are less subject to the core-hole potential.

We investigate also the effect of the electric quadrupole E_2 and magnetic dipole M_1 transitions. We found that the M_1 transitions are extremely small in comparison with the E_2 transitions and can be neglected. The E_2 transitions are two orders of magnitude smaller than electric dipole transitions E_1 (Fig. 3). Similar conclusion was derived recently by Brown *et al.*²⁵ for the XAS and XMCD spectra of the heavy rare-earth metals at the L_3 edge.

3. Fe $L_{2,3}$ and K XMCD spectra

Figure 4 shows the calculated isotropic x-ray absorption and XMCD spectra of Fe at the $L_{2,3}$ edges in the LSDA approach together with the experimental data.¹³ The LSDA theory has no difficulties in describing well the shape and intensity of the XAS and XMCD spectra, except for slight overestimation of the dichroism signal at the L_2 edge. This is a typical situation for the $3d$ transition XMCD spectra at the L_2 edge.⁴⁹

Figure 5 shows the theoretically calculated XMCD spectra at the Fe K edge in CeFe₂ using the LSDA approximation in comparison with the corresponding experimental data.³ The LSDA approach gives a quite reasonable agreement with the experiment.

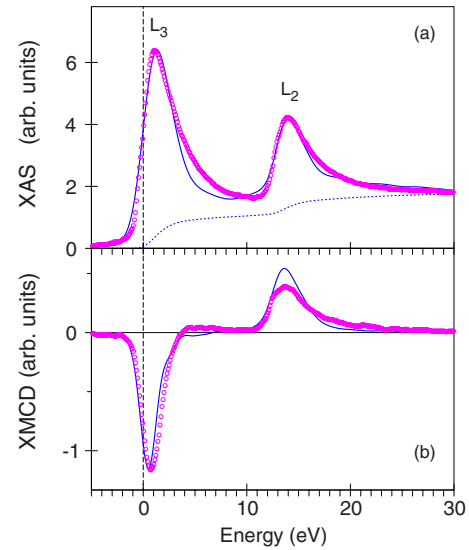


FIG. 4. (Color online) (a) Theoretically calculated by the LSDA (full line) and experimental (Ref. 13) (circles) isotropic absorption spectra of CeFe₂ at the Fe $L_{2,3}$ edges. Dotted lines show the theoretically calculated background spectra; (b) experimental (Ref. 13) (circles) XMCD spectra of CeFe₂ at the Fe $L_{2,3}$ edges in comparison with theoretically calculated ones using the LSDA approximation (full line).

The Fe $4p$ -Ce($4f, 5d$) hybridization and the spin-orbit interaction in Fe $4p$ states play crucial roles for the Fe K edge dichroism. The K XMCD spectra come from the orbital polarization in the empty p states, which may be induced by (i) the spin polarization in the p states through the spin-orbit interaction and (ii) the orbital polarization at neighboring sites through hybridization. The effect of spin-orbit interaction (SOI) and exchange splitting on the magneto-optical and the XMCD spectra of solids was studied by several authors.^{29,50–55} We calculated the K XMCD spectrum at Fe site by separately turning off the SOI of the Fe $4p$ states and of the Ce $4f$ and $5d$ states, respectively. We found that the K XMCD spectrum changes only slightly when the SOI on the

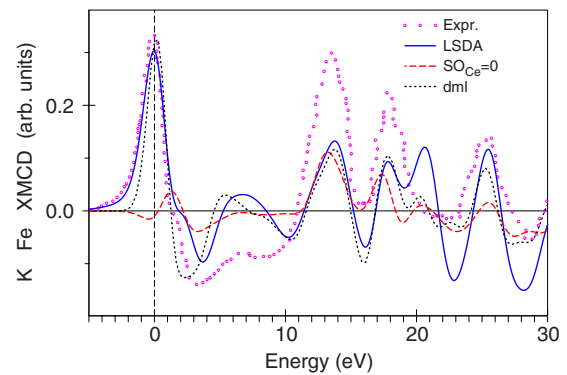


FIG. 5. (Color online) The experimental (Ref. 3) (circles) XMCD spectrum of CeFe₂ at the Fe K edge in comparison with the one calculated using the LSDA approximation (full line) and the XMCD spectrum obtained by turning off the SOI at the Ce site (dashed line); the dotted line presents the $dm_{l=1}(E)$ function (see the explanation in the text).

Fe site is turned off. While the SOI on the Ce site is turned off the prominent positive peak close to the edge almost disappears and the next negative peak at around 3.5 eV above the K edge is also reduced in intensity. This indicates that the SOI on Ce site influences the orbital mixture of Fe $4p$ states through the Fe($4p$)-Ce(d,f) hybridization. The Fe $4p$ -Ce $4f, 5d$ hybridization is responsible for large dichroism near the Fe K edge.

We also calculated the site-dependent function $dm_{it}(E) = \sum_{nk} \langle \Psi_{it}^{nk} | \hat{l}_z | \Psi_{it}^{nk} \rangle \delta(E - E_{nk})$,⁵⁶ where \hat{l}_z is the z projection of the angular momentum operator, and E_{nk} and Ψ_{it}^{nk} are the energy of the n th band and the part of the corresponding LMTO wave function formed by the states with the angular momentum l inside the atomic sphere centered at the site t , respectively. In analogy to the l -projected density of states, $dm_{it}(E)$ can be referred to as the site-projected and l -projected density of the expectation value of \hat{l}_z . As can be seen from Fig. 5 the K XMCD spectrum and $dm_{it}(E)$ function are indeed closely related to one another giving a rather simple and straightforward interpretation of the XMCD spectra at the K edge.

IV. SUMMARY

We have studied the electronic structure and x-ray magnetic circular dichroism spectra in CeFe₂ at the Ce $L_{2,3}$, $M_{4,5}$, Fe K , and $L_{2,3}$ edges using the LSDA approximation by means of an *ab initio* fully relativistic spin-polarized Dirac linear muffin-tin orbital method.

The Ce $4f$ electrons in the CeFe₂ hybridize strongly with the Fe $3d$ electrons. A large magnetic moment at the Fe site induces spin splitting of the itinerant Ce $5d$ and Ce $4f$ states

through exchange and hybridization effects. From our LSDA calculations, it has been deduced that the total moment is the result of the antiparallel coupling between Fe and cerium moments. This conclusion agrees well with the neutron-diffraction, Compton scattering, and x-ray magnetic circular dichroism experiments.

The theoretically calculated x-ray absorption spectra at the Ce $M_{4,5}$ edges have a rather simple line shape composed of two white line peaks with additional fine structures at the high-energy part of the spectra, which can be assigned to multiplet structures. The dichroism at the Ce $M_{4,5}$ edges is very large due to strong spin-orbit coupling of the initial Ce $3d$ core states and large spin polarization of the final empty $4f_{5/2,7/2}$ states.

The XAS and XMCD spectra at the Ce $L_{2,3}$ edge reflect the energy distribution and the orbital character of the Ce $5d$ bandlike states. The LSDA calculations show a good agreement in the shape of the x-ray absorption spectra at the Ce $L_{2,3}$ edges with the experimental measurements and reproduce the observed two peak structure of the Ce XMCD spectra. We investigated the influence of the electric quadrupole E_2 and magnetic dipole M_1 transitions for the Ce $L_{2,3}$ XAS and XMCD spectra. We found that the M_1 transitions are extremely small in comparison with the E_2 transitions and can be neglected. The E_2 ($2p \rightarrow 4f$) transitions are two orders of magnitude smaller than electric dipole E_1 ($2p \rightarrow 5d$) transitions.

ACKNOWLEDGMENT

V.N.A. gratefully acknowledges the hospitality at Max-Planck-Institut für Festkörperforschung in Stuttgart during his stay. This work was supported by Science and Technology Center in Ukraine (STCU), Project No. 4930.

- ¹M. S. S. Brooks and B. Johansson, in *Handbook of Magnetic Materials*, edited by K. H. J. Buschow (North-Holland, Amsterdam, 1993), Vol. 7, p. 139.
- ²J. Deportes, D. Givord, and K. Ziebeck, *J. Appl. Phys.* **52**, 2074 (1981).
- ³C. Giorgetti, S. Pizzini, E. Dartyge, A. Fontaine, F. Baudelet, C. Brouder, P. Bauer, G. Krill, S. Miraglia, D. Fruchart, and J. P. Kappler, *Phys. Rev. B* **48**, 12732 (1993).
- ⁴L. Paolasini, P. Dervenagas, P. Vulliet, J. P. Sanchez, G. H. Lander, A. Hiess, A. Panchula, and P. Canfield, *Phys. Rev. B* **58**, 12117 (1998).
- ⁵L. Paolasini, B. Ouladdiaf, N. Bernhoeft, J. P. Sanchez, P. Vulliet, G. H. Lander, and P. Canfield, *Phys. Rev. Lett.* **90**, 057201 (2003).
- ⁶H. Fukuda, H. Fujii, H. Kamura, A. Uchida, M. Kosaka, and Y. Uwatoko, *J. Magn. Magn. Mater.* **226-230**, 1200 (2001).
- ⁷T. Fujiwara, H. Fujii, Y. Ishii, S. Koiwai, M. Kosaka, Y. Uwatoko, M. Nishi, and K. Kakurai, *Physica B (Amsterdam)* **312-313**, 336 (2002).
- ⁸O. Eriksson, L. Nordstrom, M. S. S. Brooks, and B. Johansson, *Phys. Rev. Lett.* **60**, 2523 (1988).
- ⁹P. K. Khowash, *Phys. Rev. B* **43**, 6170 (1991).

- ¹⁰J. Trygg, J. M. Wills, B. Johansson, and O. Eriksson, *Phys. Rev. B* **50**, 4200 (1994).
- ¹¹T. Konishi, K. Morikawa, K. Kobayashi, T. Mizokawa, A. Fujimori, K. Mamiya, F. Iga, H. Kawanaka, Y. Nishihara, A. Delin, and O. Eriksson, *Phys. Rev. B* **62**, 14304 (2000).
- ¹²J. P. Schille, F. Bertran, M. Finazzi, C. Brouder, J. P. Kappler, and G. Krill, *Phys. Rev. B* **50**, 2985 (1994).
- ¹³A. Delobbe, A.-M. Dias, M. Finazzi, L. Stichauer, J.-P. Kappler, and G. Krill, *Europhys. Lett.* **43**, 320 (1998).
- ¹⁴M. Mizumakia, K. Yoshii, Y. Watanabe, and S. Nanaoc, *J. Appl. Crystallogr.* **408-412**, 737 (2006).
- ¹⁵F. Klose, O. Schulte, F. Rose, W. Felsch, S. Pizzini, C. Giorgetti, F. Baudelet, E. Dartyge, G. Krill, and A. Fontaine, *Phys. Rev. B* **50**, 6174 (1994).
- ¹⁶O. Gunnarsson and K. S. Schönhammer, *Phys. Rev. Lett.* **50**, 604 (1983).
- ¹⁷J. Allen, S. Oh, O. Gunnarsson, K. Schönhammer, M. Maple, M. Torikachvili, and I. Lindau, *Adv. Phys.* **35**, 275 (1986).
- ¹⁸H. Matsuyama, I. Harada, and A. Kotani, *J. Phys. Soc. Jpn.* **66**, 337 (1997).
- ¹⁹K. Fukui, H. Matsuyama, I. Harada, J. C. Parlebas, and A. Kotani, *J. Electron Spectrosc. Relat. Phenom.* **104**, 67 (1999).

- ²⁰K. Asakura, K. Fukui, H. Ogasawara, I. Harada, J. C. Parlebas, and A. Kotani, *J. Phys. Soc. Jpn.* **73**, 2008 (2004).
- ²¹J. C. Parlebas and A. Kotani, *J. Electron Spectrosc. Relat. Phenom.* **136**, 3 (2004).
- ²²K. Asakura, A. Kotani, and I. Harada, *J. Phys. Soc. Jpn.* **74**, 1328 (2005).
- ²³J. Parlebas, K. Asakura, A. Fujiwara, I. Harada, and A. Kotani, *Phys. Rep.* **431**, 1 (2006).
- ²⁴V. Antonov, B. Harmon, and A. Yaresko, *Electronic Structure and Magneto-Optical Properties of Solids* (Kluwer, Dordrecht, 2004).
- ²⁵S. D. Brown, P. Strange, L. Bouchenoire, B. Zarychta, P. B. J. Thompson, D. Mannix, S. J. Stockton, M. Horne, E. Arola, H. Ebert, Z. Szotek, W. M. Temmerman, and D. Fort, *Phys. Rev. Lett.* **99**, 247401 (2007).
- ²⁶B. N. Harmon and V. N. Antonov, *J. Appl. Phys.* **93**, 4678 (2003).
- ²⁷P. Mavropoulos, M. Lezaic, and S. Blugel, *Phys. Rev. B* **72**, 174428 (2005).
- ²⁸Y. Lee, B. N. Harmon, A. I. Goldman, and J. C. Lang, *J. Appl. Phys.* **101**, 09G525 (2007).
- ²⁹K. Takahashi, *Phys. Rev. B* **76**, 184422 (2007).
- ³⁰O. Guillot-Noel, P. Goldner, Y. L. Du, E. Baldit, P. Monnier, and K. Bencheikh, *Phys. Rev. B* **74**, 214409 (2006).
- ³¹M. Forsthuber, F. Lehner, G. Wiesinger, G. Hilscher, T. Huber, E. Gratz, and G. Wortmann, *J. Magn. Magn. Mater.* **90**, 471 (1990).
- ³²V. N. Antonov, O. Jepsen, A. N. Yaresko, and A. P. Shpak, *J. Appl. Phys.* **100**, 043711 (2006).
- ³³V. N. Antonov, B. N. Harmon, O. Andryushchenko, L. Bekenev, and A. N. Yaresko, *Low Temp. Phys.* **30**, 305 (2004).
- ³⁴O. K. Andersen, *Phys. Rev. B* **12**, 3060 (1975).
- ³⁵V. V. Nemoshkalenko and V. N. Antonov, *Computational Methods in Solid State Physics* (Gordon and Breach, Amsterdam, 1998).
- ³⁶J. P. Perdew and Y. Wang, *Phys. Rev. B* **45**, 13244 (1992).
- ³⁷P. E. Blöchl, O. Jepsen, and O. K. Andersen, *Phys. Rev. B* **49**, 16223 (1994).
- ³⁸F. K. Richtmyer, S. W. Barnes, and E. Ramberg, *Phys. Rev.* **46**, 843 (1934).
- ³⁹F. Leuenberger, A. Parge, W. Felsch, F. Baudelet, C. Giorgetti, E. Dartyge, and F. Wilhelm, *Phys. Rev. B* **73**, 214430 (2006).
- ⁴⁰J. Röhler, *J. Magn. Magn. Mater.* **47-48**, 175 (1985).
- ⁴¹J. L. Campbell and T. Parr, *At. Data Nucl. Data Tables* **77**, 1 (2001).
- ⁴²S. J. Kennedy and B. R. Coles, *J. Phys.: Condens. Matter* **2**, 1213 (1990).
- ⁴³S. J. Kennedy, P. J. Brown, and B. R. Coles, *J. Phys.: Condens. Matter* **5**, 5169 (1993).
- ⁴⁴M. J. Cooper, P. K. Lawson, M. A. G. Dixon, E. Zukowski, D. N. Timms, F. Itoh, H. Sakurai, H. Kawata, Y. Tanaka, and M. Ito, *Phys. Rev. B* **54**, 4068 (1996).
- ⁴⁵J. Zaanen, G. A. Sawatzky, J. Fink, W. Speier, and J. C. Fuggle, *Phys. Rev. B* **32**, 4905 (1985).
- ⁴⁶J. Schwitalla and H. Ebert, *Phys. Rev. Lett.* **80**, 4586 (1998).
- ⁴⁷P. Krüger and C. R. Natoli, *Phys. Rev. B* **70**, 245120 (2004).
- ⁴⁸A. L. Ankudinov, A. I. Nesvizhskii, and J. J. Rehr, *Phys. Rev. B* **67**, 115120 (2003).
- ⁴⁹V. N. Antonov, A. P. Shpak, and A. N. Yaresko, *Low Temp. Phys.* **34**, 1 (2008).
- ⁵⁰J. I. Igarashi and K. Hirai, *Phys. Rev. B* **50**, 17820 (1994).
- ⁵¹S. Uba, L. Uba, A. Y. Perlov, A. N. Yaresko, V. N. Antonov, and R. Gontarz, *J. Phys.: Condens. Matter* **9**, 447 (1997).
- ⁵²M. Takahashi and J. I. Igarashi, *Phys. Rev. B* **67**, 245104 (2003).
- ⁵³M. Usuda, J. I. Igarashi, and A. Kodama, *Phys. Rev. B* **69**, 224402 (2004).
- ⁵⁴V. N. Antonov, B. N. Harmon, A. N. Yaresko, and A. P. Shpak, *Phys. Rev. B* **75**, 165114 (2007).
- ⁵⁵V. Antonov, B. Harmon, and A. Yaresko, *J. Phys.: Condens. Matter* **19**, 186222 (2007).
- ⁵⁶L. Uba, S. Uba, V. N. Antonov, A. N. Yaresko, T. Slezak, and J. Korecki, *Phys. Rev. B* **62**, 13731 (2000).